Published in final edited form as:
J Neurosurg Spine. 2009 June ; 10(6): . doi:10.3171/2009.2.SPINE08391.

An orthotopic murine model of human spinal metastasis: histological and functional correlations

Claudio E. Tatsui, M.D., **Frederick F. Lang, M.D.**, **Joy Gumin, B.S.**, **Dima Suki, Ph.D.**, **Naoki Shinojima, M.D.**, and **Laurence D. Rhines, M.D.**
Department of Neurosurgery, The University of Texas M. D. Anderson Cancer Center, Houston, Texas

Abstract

Object—There is currently no reproducible animal model of human spinal metastasis that allows for laboratory study of the human disease. Consequently, the authors sought to develop an orthotopic model of spinal metastasis by using a human lung cancer cell line, and to correlate neurological decline with tumor growth.

Methods—To establish a model of spinal metastasis, the authors used a transperitoneal surgical approach to implant PC-14 lung tumors into the L-3 vertebral body of nude mice via a drill hole. In 24 animals, motor function was scored daily by using the validated semiquantitative Basso-Beattie-Bresnahan (BBB) scale. A second group of 26 animals (6 or 7 per time point) were sacrificed at specific times, and the spines were removed, sectioned, and stained. Canal compromise was analyzed quantitatively by determining the ratio of the area of the neural elements to the area of the spinal canal on histological sections (neural/canal ratio). Correlations between BBB score and histological evaluation of tumor growth were assessed.

Results—Lung cancer xenografts grew in all animals undergoing functional evaluation (24 mice) according to a reliable and reproducible time course, with paraplegia occurring at a median interval of 30 days following tumor implantation (95% CI 28.1–31.9 days). Importantly, the analysis defined 4 key milestones based on components of the BBB score; these were observed in all animals, were consistent, and correlated with histological progression of tumor. From Days 1 to 14, the mean BBB score declined from 21 to 19. The animals progressed from normal walking with the tail up to walking with the tail constantly touching the ground (milestone 1). The median time to tail dragging was 12 days (95% CI 10.8–13.2). Histological studies on Day 14 demonstrated that tumor had progressed from partial to complete VB infiltration, with initial compression of the neural elements and epidural tumor extension to adjacent levels (mean neural/canal ratio 0.32 ± 0.05, 7 mice). From Days 15 to 20/21 (left/right leg), the mean BBB score declined from 19 to 14. Animals showed gait deterioration, with the development of dorsal stepping (milestone 2). The median time to dorsal stepping was 21 days (95% CI 19.4–22.6) in the left hindlimb and 23 days (95% CI 20.6–25.4) in the right hindlimb. Histological studies on Day 21 demonstrated an increase in the severity of the neural element compression, with tumor extending to adjacent epidural and osseous levels (mean neural/canal ratio 0.19 ± 0.05, 6 mice). From Days 22 to 26/27 (left/right leg), the mean BBB score declined from 14 to 8. Animals had progressive difficulty ambulating, to the point where they showed only sweeping movements of the hindlimb (milestone 3). The median time to hindlimb sweeping was 26 days (95% CI 23.6–28.4) and 28 days (95% CI 27.1–28.9) in the left and right hindlimbs, respectively. Histological

Address correspondence to: Frederick F. Lang, M.D., Department of Neurosurgery, M. D. Anderson Cancer Center, 1515 Holcombe Boulevard, Box 442, Houston, Texas. 77030. flang@mdanderson.org..

Disclosure The authors report no other conflicts of interest concerning the materials or methods used in this study or the findings specified in this paper.

studies on Day 28 revealed progressive obliteration of the spinal canal (mean neural/canal ratio 0.09 ± 0.01, 7 mice). From Days 29 to 36, the animals progressed to paralysis (milestone 4). The median time to paralysis was 29 days (95% CI 27.6–30.4) and 30 days (95% CI 28.1–31.9) in the left and right hindlimbs, respectively.

Conclusions—The authors have developed an orthotopic murine model of human spinal metastasis in which neurological decline reproducibly correlates with severity of tumor progression. Although developed for lung cancer, this model can be expanded to study other types of metastatic or primary spinal tumors. Ultimately, this will allow testing of targeted therapies against specific tumor types.

Keywords

spinal metastasis; nude mouse; spinal cord compression; animal model

Metastases to the spine are a major source of pain and disability in patients with cancer. Spinal cord compression secondary to spinal metastases occurs in up to 14% of all cancer patients, with an incidence of > 20,000 cases per year in the US.[10] Among the malignancies that metastasize to the spine, lung cancer is one of the most aggressive, with a 1-year survival rate of ~ 22%.[12]

Surgery and/or radiation are the current primary treatments for spinal metastases. Unfortunately, local recurrence is common, and therapeutic options after recurrence are often limited. Clearly, there is an urgent need for the development of novel, more effective treatment modalities. However, advances in this field have been hindered by the lack of adequate animal models of the human disease.

The ideal model for evaluating therapeutic treatments should mimic the human disease. It should be developed from human cancer cells, should be reproducible, and neurological decline should correlate with the severity of spinal cord compression. In this context, Arguello et al.[2] reported a nude mouse model in which intracardiac injection of tumor cells resulted in spinal metastases. Although human tumor cells were used, the location and number of metastases were unpredictable, and thus the disease course was not reproducible, making it difficult to assess therapeutic interventions. In contrast, Mantha et al.[8] recently described a rat model in which tumors from a rat breast cancer cell line were implanted in a lumbar VB. Although the location of the metastasis could be predicted and the model was reproducible, reliance on a syngeneic rat cancer cell line precludes evaluation of therapies directed against human tumors. Importantly, in neither of the models were histological correlates of clinical deterioration evaluated over time so that the neurological examination could be used to guide when to begin a therapy or to determine whether a therapy was effective based on end points other than paraplegia or death.

To address this need, we now report the development of an orthotopic nude mouse model in which the human lung adenocarcinoma cell line PC-14 was used. We show that implantation of PC-14 tumors into the VB of the nude mouse is feasible, despite the small size of the animal. More importantly, we demonstrate that progressive neurological decline occurs within a reproducible time frame, and that specific changes in the neurological examination correlate with the severity of spinal cord compression. This model can be extended to other tumor histological types, and it is anticipated that this will provide an avenue to explore novel therapies against specific spinal tumor types.

Methods

Animal Preparation

Athymic nude mice weighing between 30 and 40 g were purchased from the Animal Reproduction Area of the National Cancer Institute–Frederick Cancer Research and Development Center. Animals were housed in standard facilities, 5 mice per cage, with free access to water and rodent chow. During procedures animals were anesthetized with a solution of ketamine hydrochloride (25 mg/ml) and xylazine (2.5 mg/ml) via an intraperitoneal injection at a volume of 100 μl/10 g body weight. All animal manipulations were performed in accordance with institutional guidelines under approved protocols.

Cell Culture

The lung adenocarcinoma cell line PC-14 was a gift from Dr. Suyun Huang (M. D. Anderson Cancer Center), and was maintained in culture with RPMI 1640 Cellgro medium (Mediatech, Inc.) with 10% fetal bovine serum, penicillin (base 80.5 U/ml), and streptomycin (80.5 pg/ml) (all from Gibco BRL) in a humidified incubator with 5% CO_2/95% room air at 37°C.

Development of a Subcutaneous Xenograft of Human Lung Adenocarcinoma Cells

Monolayers of PC-14 cells were detached by trypsinization, washed, and suspended in phosphate-buffered saline at a concentration of 10^6 cells per 100 μl. Carrier animals were anesthetized and 300 μl of the cell suspension was injected subcutaneously into the flank. Approximately 28 days after injection, anesthesia was induced in the carrier animals and subcutaneous tumors measuring 10 × 10 mm were harvested by dissection, placed in a culture dish with RPMI 1640 plus 10% fetal bovine serum, and maintained at room temperature until implanted in the VB of the experimental animals. After tumor harvesting, the carrier animals were euthanized by CO_2 inhalation, in accordance with animal facility protocols.

Development of the Intravertebral Tumor

Animals were anesthetized and placed supine on a heating pad with their limbs affixed to the pad with tape. The abdomen was prepared with a chlorhexidine swab, and a 1.5-cm midline abdominal skin incision was made with a No. 15 scalpel blade. The underlying abdominal muscles were exposed and elevated to separate the bowels from the abdominal wall. An incision between the 2 rectus abdominis muscles was extended from 5 mm above the pubic arch until the inferior border of the liver could be identified. The abdominal muscles were gently retracted laterally with fishhooks. The small and large intestines were mobilized to the right and left side of the peritoneal cavity and held gently with blunt fishhooks. At this point, the inferior pole of the left kidney was identified, and the posterior peritoneal membrane on the left side was incised between the ureter and the vascular bundle containing the aorta and the vena cava. Using a fine Dumont forceps and microscissors, the vascular bundle was dissected on the left side and mobilized to the right to expose the underlying psoas muscle and VBs. The left psoas muscle was dissected with a fine periosteal elevator and retracted laterally. Venous bleeding at this stage was controlled with simple compression with cotton balls for 30 seconds. Mobilization of the psoas muscle immediately caudal to the inferior pole of the left kidney exposed the L-3 VB (Fig. 1). Using a 1-mm bur hand drill placed at an angle of 45° with the bone surface, a hole was created in the middle of the exposed vertebra to a depth of 2 mm. At this point, a piece of the previously harvested tumor (~ 0.5 × 0.5 mm) was inserted into the VB. The hole was then sealed with a PMMA plug (Stryker) as described by Mantha et al.[8] After the hole was sealed, the bowels were

gently returned to the original position, and the abdominal muscles and the skin were closed in a single layer with a running 3–0 silk suture (Ethicon).

Functional Assessment

Neurological function was graded according to the method described by Basso et al.[4] (the BBB scale), in criteria, where 21 is the highest (normal function) and 0 (plegia) is the lowest score. In brief, the mouse was placed in an open field, and its gait was observed for 4 minutes. We used a plastic wading pool with a smooth floor measuring 90 cm in diameter with a 15-cm wall height to obtain reproducible results. The scores for the 24 animals were averaged daily and plotted graphically to demonstrate neurological decline over the course of the study.

Tissue Processing

Histological analyses were performed on subsets of animals by using standard methods. Briefly, the spines were harvested, fixed in 10% formalin for 24 hours, and then placed in decalcifying solution for 1–2 days. When the bone was soft, the specimen was dissected with the aid of a surgical microscope and the PMMA plug was carefully removed so as not to damage the surrounding tissues. The spines were embedded in paraffin, sectioned at a thickness of 10 μm, and stained with H & E.

Analysis of Neural Compression

Histological sections obtained in mice sacrificed at 7, 14, 21, and 28 days after tumor implantation were analyzed at a magnification of 50. Imaging software (ImagePro; Media Cybernetics, Inc.) was used to measure the area of the spinal canal (canal area) and the area of the spinal cord and nerve roots (neural area) at the level of tumor implantation. The ratio of the neural area to the canal area was used as a measure of neural compression. This ratio was measured in 26 animals (6 or 7 per time point), and the mean ± SEM at each time point was plotted.

Statistical Analysis

The means and their standard errors (expressed as the mean ± SEM) were obtained. Differences between the mean neural/canal ratios at the 4 time points were assessed using a 1-way analysis of variance with a Bonferroni correction for multiple comparisons. The Kaplan-Meier method was used to estimate the medians and 95% CIs for all time-to-event variables.

Results

Tumor Engraftment and Survival Analysis

A pilot study was performed in 15 animals to assess the feasibility of our model. Significant left leg weakness was observed immediately after the surgical procedure in all animals, and the left hindlimb was completely paralyzed in the majority. These animals were sacrificed 3 and 5 days after tumor implantation, and analysis of the fixed specimens confirmed that tumor engraftment had begun in all animals, and that the cancer cells were contained entirely in the marrow of the VB without extension into the epidural space or around the nerve roots. Given these initial results, and because the weakness was immediate, we assumed that the deficits were due to local trauma and sought to minimize this. A sham experiment with 2 animals was conducted in which surgery without tumor implantation was performed. The same surgical technique was used, but the dissection of the iliopsoas muscle was limited to the vertebral surface, and the size of the PMMA plug was reduced. These animals recovered from surgery without neurological deficits and remained asymptomatic

for > 60 days after the procedure. Therefore, weakness observed immediately after surgery in the initial cohort was attributed to overmanipulation of the iliopsoas muscle and the insertion of an excessive amount of PMMA to plug the hole, causing pressure on the adjacent muscle and nerves. This was corrected in subsequent experiments by minimizing dissection of the muscle and by reducing the size of the PMMA plug.

Subsequently, 3 identical experiments, each using 10 animals, were performed. Four animals in the first experiment died before the onset of paraplegia (BBB scores were 17, 16, 14, and 10, respectively) due to neurogenic bladder (2 died on Day 19 after implantation, 1 on Day 26, and 1 on Day 27). All 4 of these animals were found to have tumor engraftment on histological evaluation, but they were excluded from the functional analysis. These deaths alerted us to the fact that animals can develop neurogenic bladder as early as 19 days after tumor implantation, and thus require daily manual bladder expression. This method drastically reduced complications of bladder dysfunction in the remaining 26 animals that were followed for neurological function. Of these, only 2 other animals had to be excluded from the functional analysis. This was due to clogging of the urethra, leading to bladder distention that could not be resolved with manual expression. In the remaining 24 mice, complete paraplegia occurred at a median interval of 30 days following tumor implantation (95% CI 28.1–31.9 days) and mandated sacrifice of the animals. Tumor engraftment was verified in all animals at the time of death.

Functional Analysis

Twenty-four animals were observed daily for neurological function of their hindlimbs, and they were assessed using the BBB scale. The mean BBB scores declined progressively over time (Fig. 2). More importantly, careful observation of the animals revealed that 4 key milestones of the BBB scoring system were easily identified and occurred in a highly reproducible manner (Tables 1 and 2).

A normal mouse walks with the tail off of the ground and with coordinated steps between forelimb and hindlimb. The plantar surface of the paw touches the ground with every step. In this context, the first observable change in function was the inability of animals to maintain a tail-up position. Instead, animals ambulated with the tail continuously on the ground (BBB score of 19; Table 1). When normal animals are held off the ground by the dorsal skin, the tail spins with circular movement above the level of the head. Loss of muscle tone of the tail was confirmed by the inability of the animal to spin the tail when grabbed by the dorsal skin. The occurrence of tail dragging (milestone 1) due to tail weakness was easily observed and occurred at a median interval of 12 days after the surgery (95% CI 10.8–13.2; Table 2). A normal stepping cycle involves weight support through the plantar surface of the paws, followed by forward limb advancement with the toes completely clearing any contact with the ground, and then reestablishment of plantar weight support. The second major neurological change observed in our model was that toe clearance off the ground became inconsistent, and progressed to the point of inability to reestablish contact of the plantar surface of the paw with the ground at the end of the cycle. Instead, animals developed a characteristic “dorsal step” (milestone 2), in which the dorsal surface of the foot hit the ground (BBB score of 14; Table 1). The median time to observe this gait pattern in the left and right hindlimbs was 21 days (95% CI 19.4–22.6) and 23 days (95% CI 20.6–25.4) after tumor implantation, respectively (Table 2).

With time, the frequency of dorsal stepping increased, and eventually animals walked with a lateral rotation of the paws that progressed to loss of weight support. The animals then began to sweep the hindlimb rather than lift it (BBB score of 8; Table 1). Forward advancement became increasingly dependent on the action of the forelimbs. This hindlimb sweeping (milestone 3) occurred at a median time of 26 days (95% CI 23.6–28.4) and 28

days (95% CI 27.1–28.9) following tumor implantation, in the left and right hindlimbs, respectively (Table 2).

Finally the hindlimb dysfunction progressed to the point of complete paralysis (BBB score of 0; Table 1). Paraplegia (milestone 4) occurred at a median interval of 29 days (95% CI 27.6–30.4) and 30 days (95% CI 28.1–31.9) after tumor implantation, in the left and right hindlimbs, respectively (Table 2). All animals with this grade of dysfunction had to be sacrificed, in accordance with the guidelines of the Animal Care and Use Committee of our institution. The time from tumor implantation to the onset of each of these critical neurological milestones is summarized in Table 2.

Histological Analysis

Understanding the histological changes in the spine after tumor implantation required a working knowledge of normal mouse spinal anatomy. Histological examination of the normal nude mouse spine (5 animals) revealed anatomical elements similar to those of the human spine. The 6 lumbar vertebrae were triangular in shape and separated by intervertebral discs. Each vertebra had recognizable pedicles, lamina, and spinous and transverse processes. All levels were composed of cancellous bone with a cortical shell. Importantly, within the cancellous bone there were vascular channels that communicated with the IVP posterior to the VB (equivalent to the Batson plexus) via osseous foramina (Fig. 3A and B). The IVP extended to adjacent levels in the epidural space.

To correlate functional decline with tumor growth, histological analyses were performed in 26 animals. Six or 7 mice were sacrificed at each of 4 time points after tumor implantation (Days 7, 14, 21, and 28). The animals sacrificed on Day 7 were neurologically normal. The other 3 time points roughly correlated with the advent of tail dragging (Day 14), dorsal stepping (Day 21), and hindlimb sweeping (Day 28), respectively. Specimens were analyzed semiquantitatively for the degree of tumor infiltration within the vertebra, compression of the nerve roots, compression of the spinal cord, and extension of tumor to adjacent levels (Table 3). To quantify the degree of neural element compression more precisely, the area of the spinal canal (canal area) and the area of the identified spinal cord and nerve roots within the spinal canal (neural area) were measured. The “neural/canal ratio” was then calculated by dividing the neural area by the canal area. The mean ± SEM of these measurements at each time point was determined. This method is illustrated in Fig. 4, and results are depicted graphically in Fig. 5.

Histological analysis of the spines removed from neurologically normal animals 7 days after tumor implantation (6 mice) demonstrated tumor cells infiltrating the L-3 VB. In these cases normal trabecular bone was evident in most areas (Fig. 6). Tumor cells could be seen infiltrating the venous foramina that connect the marrow to the epidural venous plexus (Fig. 3C–E and Fig. 6B–D). Early encroachment into the epidural space was evident, causing partial compression of the nerve roots. At this stage, the tumor remained localized at the level of implantation. The mean neural/canal ratio was 0.48 ± 0.03. This value corresponded with a subjective rating of “no” cord compression (Table 3, Fig. 5).

Animals sacrificed 14 days after tumor implantation (7 mice), shortly after the development of tail dragging, demonstrated tumor cells within the entire L-3 VB. In addition, tumor cells could be seen infiltrating much of the posterior elements bilaterally, but the shape of the spinous and transverse processes was still intact. There was substantial destruction of the trabecular bone. The mean neural/canal ratio decreased to 0.32 ± 0.05, and we observed increased nerve root encasement and canal compromise (Table 3). This degree of neural element compression was significantly different when compared with Day 7 ($p = 0.04$; Fig. 5). This value corresponded to a subjective rating of “mild” cord compression at this time

point. In addition, there was evidence of epidural, but not osseous, extension to adjacent levels (Fig. 7).

Histological studies of the spines of animals sacrificed on Day 21 following tumor implantation (6 mice) are shown in Fig. 8. These animals were just developing dorsal stepping at the time of planned death. The mean neural/canal ratio decreased to 0.19 ± 0.05 (Table 3). This degree of compression was statistically significantly different compared with Day 7 ($p < 0.001$; Fig. 5). This value corresponded to a subjective rating of “severe” spinal cord compression. In addition, we observed significant bone destruction, with extension of tumor into the epidural space and VBs of the adjacent levels.

Analysis of the spines of mice sacrificed 28 days after tumor implantation (7 mice), when animals generally developed hindlimb sweeping that progressed rapidly to paraplegia, showed complete destruction of the trabecular bone of the implanted VB. At this point, the mean neural/canal ratio was 0.09 ± 0.01 (Table 3). This degree of neural element compromise was statistically significantly different compared with Day 7 ($p < 0.001$; Fig. 5). In most specimens the spinal canal was obliterated by tumor, making the spinal cord and nerves difficult to identify (Fig. 9).

Discussion

We describe a nude mouse model of spinal metastasis that is reproducible and derived from human cancer cells. Specifically, we show that xenografts of human lung cancer can be established in a single lumbar VB (L-3) of nude mice, and that these xenografts grow in a histologically predictable pattern that results in a consistent, progressive decline in hindlimb neurological function. This model is valuable because it represents an orthotopic model of the human disease, and thus can be used for evaluating novel therapeutic approaches developed specifically for spinal metastases.

Our model has advantages over other spinal metastasis models that have been described heretofore.[1,2,8,9,11,13] Arguello et al.[2] established a nude mouse model that relied on intracardiac injection of tumor cells for the establishment of spinal metastases. This model had the advantage of using human tumor cells, but suffered from the fact that the location and number of metastases were unpredictable. Therefore, the progression of neurological decline was not reproducible, making it difficult to assess therapeutic interventions. To overcome this problem, Mantha et al.[8] directly implanted tumors into the lumbar VBs of rats, thereby establishing a predictable location of the tumor. Unfortunately, these investigators used tumors derived from a rat breast cancer cell line. This choice of a nonhuman cell type raises concerns about the applicability of this model in the study of human cancers. Consequently, our model combines the advantages of both of these models and eliminates their shortcomings. Like Arguello and colleagues,[2,3] we use cells derived from human tumors, and like Mantha et al., we directly implant these tumor cells into the VB. However, in contrast to Mantha et al., we rely on immunocompromised nude mice, which allows for the establishment of human xenografts. Although the VBs of nude mice are smaller than those in rats, making the implantation more technically challenging, we show that xenografting of the VBs of nude mice is possible, although our pilot studies showed that great care must be taken with the iliopsoas muscle dissection and that limiting the size of the PMMA plug was necessary. Although nude rats can be used, nude mice are easier to handle, and are significantly less expensive, so that larger numbers of subjects can be tested.

Although we used PC-14 human lung cancer cells in the described studies, in fact any human cell type can be implanted in our model. This is important for metastatic tumors, because the biological behavior and response to therapy of spinal metastases varies

depending on the type of primary tumor. For example, the 1-year survival rate for patients with spinal metastases from breast cancer is 78%, whereas that from lung cancer is only 22%,[12] denoting the heterogeneity of the biological properties of different malignancies. Thus it cannot be assumed that models of one cancer type are applicable to another type. Separate models of each tumor type would be advantageous and can be achieved with the model described here. Of additional interest is that primary tumors of the spine can also be used in this model. Indeed, in vivo models of primary tumors such as human chordomas, chondrosarcomas, osteogenic sarcomas, and so forth can be studied. Establishing these models would be of obvious advantage for developing therapeutic strategies directed against these rare diseases.

Correlation of histological tumor progression with neurological deterioration is a unique aspect of our experimental model of spinal metastasis. Specimens obtained at Days 7 and 14 confirmed that tumor initially contained within the bone marrow of the VB gained access to the epidural space. By measuring the area within the spinal canal occupied by the neural elements, and dividing this value by the area of the spinal canal itself, we created an index reflective of canal compromise. Progressive decrease in the neural/canal ratio corresponded to progressive decline in the space available for the neural elements due to tumor progression. This ratio decreased over time, and we found significant differences between the values obtained at 7 days versus 14, 21, and 28 days after tumor implantation (Table 3, Fig. 5). To our knowledge, this analysis represents the first quantitative assessment of tumor progression over time in an animal model of spinal cord compression. It is of value because it provides a quantitative means of assessing future strategies for treating spinal metastases in this model.

Another important aspect of our study is that we establish specific and easily observable major neurological events that demarcate points in the progression of the disease and that have direct anatomical correlates of spinal cord compression. Specifically, we found 4 consistently occurring milestones; that is, tail dragging, dorsal stepping, hindlimb sweeping, and paraplegia. Each of these correlated with progressive neural element compression (Figs. 7–9). These neurological milestones are of value because they can be easily tracked and compared between animals. The most critical was the identification of tail dragging, which not only documented tumor engraftment, but also simulated the human condition where tumor burden was limited. In this context, we suggest that this easily observable event might be used as a time point for starting therapeutic interventions. The efficacy of a therapy can then be evaluated over time by comparing the onset of the later neurological events in treated and nontreated animals. This is important because these observable end points reduce the requirement for imaging (for example, MR imaging) to document the presence and progression of tumor.

In addition, we believe that the observed events reported here are more reliable indicators of clinical progression than the BBB score, which has been previously used by Mantha et al.[8] Although Basso et al.[5] reported a scoring system to evaluate the posttraumatic recovery of neurological function in mice (the BMS), we chose to evaluate neurological function using the BBB score, which was developed for rats. Our decision to use the BBB scale was based first on the fact that Mantha et al. had used this score in their study, and we sought to compare our model to their model. Second, the BBB score (composed of 21 points) offered us more flexibility in grading neurological decline than the BMS score (composed of only 9 points). In fact, hindlimb sweeping, one of our consistent milestones, is not a component of the BMS. It must be noted that both the BBB and the BMS scoring systems were originally developed to evaluate the recovery of neurological function in animal models of spinal cord contusion. Our paper examines neurological decline caused by epidural spinal cord compression, an opposite sequence of events with a very different mechanism of injury. In

our spinal tumor model, animals progress from normal to abnormal function, and the BBB scale is, therefore, used to grade neurological function progressing in the reverse order of the spinal cord injury models for which the scale was originally developed. Indeed, some of the events described in the recovery of function after spinal cord injury are not obvious during neurological decline from tumor progression, and it was often difficult to define with precision the scores ranging between 9 and 18. Because of these problems, we conclude that the timing of the 4 major neurological milestones described here may be a more useful functional outcome measure. These events correlate with the BBB score (see Table 1). We propose that the 4 neurological milestones of tail dragging, dorsal stepping, hindlimb sweeping, and paralysis replace BBB or BMS scores in future studies of spinal cord compression caused by tumor growth in these animal models.

Another important clinical symptom that was reproduced in our model was sphincter dysfunction, represented by the development of neurogenic bladder. This feature occurred after the observation of tail dragging. We noted that the bladder was atonic and distended, suggesting compression of the conus medullaris. Once bladder dysfunction occurred, gentle manual expression was required on a daily basis. If the bladder was not completely emptied, the residual urine became yellow, and cellular debris clogged the urethra, making the bladder expression more difficult (and in rare cases impossible). This observation was obtained from the 4 animals that died due to unrecognized neurogenic bladder, and from the 2 animals in which we were unable to express the urine. These animals had to be euthanized due to signs of pain and distress.

Our model is also of interest because it provides some insight into the biological steps that occur during progression of spinal metastases, and thus may allow for study of the molecular interactions between the tumor cells, the VB vasculature, and the bone and marrow microenvironment. One of the more interesting findings in our histological analyses was the role of the venous foramina, which are located within the posterior wall of the VB, and through which venous channels connect the VB vasculature with the epidural venous plexus (Batson plexus). It has been postulated that metastastic tumors reach the VB via this epidural venous plexus.[6] When labeled tumor cells are injected in the tail vein after the inferior vena cava is clamped, these cells can be found inside the VBs and in the epidural space.[7] Thus, transitory venous reflux associated with peaks of high intrathoracic or intraabdominal pressure may allow tumor cells to reach the VB via this epidural plexus.[6] However, in the human disease, bone infiltration often precedes epidural extension, suggesting that tumor cells reach the VB via antegrade flow through arterial channels. Consistent with this observation, Arguello et al.[2] established vertebral metastases via intracardiac injection of tumor cells, and these cells then caused epidural compression. In this context, our studies confirm the findings of Arguello and colleagues.[2,3] Specifically, in our model the bone marrow is infiltrated before destruction of the trabecular bone, indicating that the marrow is a fertile soil for metastatic cells. Moreover, once tumor cells are established in the VB, our studies indicate that the venous foramina act as conduits for antegrade movement of the tumor cells into the epidural space, because these foramina represent weak points in the posterior wall of the vertebrae. Interestingly, this pathway permitted extension of the tumor into the epidural space before the development of complete VB destruction. Thus, the PC-14 cells proliferated in the medullary bone, replacing the hematopoietic bone marrow and gaining access to the venous channels inside the VB. The posterior venous foramina allowed the tumor cells to exit the VB and to enter the epidural space. In addition, the anterior foramina allowed the tumor cells to extend into the retroperitoneum via a similar mechanism. Once within the epidural space, tumor cells extended superiorly and inferiorly to adjacent levels and entered the VBs of these levels via the posterior venous channels. These channels allowed access to the marrow without destruction of the trabecular bone. Consistent with the idea that the bone marrow is a fertile soil for tumor growth, signals from

the bone marrow probably increase the propensity of the cells to enter the marrow and move from the epidural space. Interestingly, this progression to adjacent levels occurs without the destruction of the intravertebral disc, which is the pattern seen clinically.[2]

Conclusions

We conclude that our model provides a reliable correlation between tumor progression and neurological deterioration. The pattern of colonization of the VB is highly reproducible, and this methodology can be expanded to other human cell lines (breast, prostate, and kidney). The ability to follow the tumor progression and compression of the spinal cord clinically will allow this model to be used to study and compare different treatment strategies.

Acknowledgments

This study was supported by grants from the National Institutes of Health/National Cancer Institute (Grant Nos. CA115729 and P50 CA127001), a grant from the National Brain Tumor Foundation, and by the Elias Family Fund for Brain Tumor Research, the Gene Pennebaker Brain Cancer Research Fund, the Marcus Foundation, and the Brian McCulloch Research Fund (all to Dr. Lang). Dr. Rhines received an M. D. Anderson Cancer Center Institutional Research Grant.

Abbreviations used in this paper

BBB	Basso-Beattie-Bresnahan
BMS	Basso Mouse Scale
IVP	internal venous plexus
PMMA	polymethylmethacrylate
VB	vertebral body

References

1. Amundson E, Pradilla G, Brastianos P, Bagley C, Riley LH III, Garonzik IM, et al. A novel intravertebral tumor model in rabbits. Neurosurgery. 2005; 57:341–346. [PubMed: 16094165]
2. Arguello F, Baggs RB, Duerst RE, Johnstone L, McQueen K, Frantz CN. Pathogenesis of vertebral metastasis and epidural spinal cord compression. Cancer. 1990; 65:98–106. [PubMed: 2293874]
3. Arguello F, Baggs RB, Frantz CN. A murine model of experimental metastasis to bone and bone marrow. Cancer Res. 1988; 48:6876–6881. [PubMed: 3180096]
4. Basso DM, Beattie MS, Bresnahan JC. A sensitive and reliable locomotor rating scale for open field testing in rats. J Neurotrauma. 1995; 12:1–21. [PubMed: 7783230]
5. Basso DM, Fisher LC, Anderson AJ, Jakeman LB, McTigue DM, Popovich PG. Basso Mouse Scale for locomotion detects differences in recovery after spinal cord injury in five common mouse strains. J Neurotrauma. 2006; 23:635–659. [PubMed: 16689667]
6. Batson OV. The function of the vertebral veins and their role in the spread of metastases. Ann Surg. 1940; 112:138–149. [PubMed: 17857618]
7. Harada M, Shimizu A, Nakamura Y, Nemoto R. Role of the vertebral venous system in metastatic spread of cancer cells to the bone. Adv Exp Med Biol. 1992; 324:83–92. [PubMed: 1492628]
8. Mantha A, Legnani FG, Bagley CA, Gallia GL, Garonzik I, Pradilla G, et al. A novel rat model for the study of intraosseous metastatic spine cancer. J Neurosurg Spine. 2005; 2:303–307. [PubMed: 15796355]
9. Miki T, Yano S, Hanibuchi M, Sone S. Bone metastasis model with multiorgan dissemination of human small-cell lung cancer (SBC-5) cells in natural killer cell-depleted SCID mice. Oncol Res. 2000; 12:209–217. [PubMed: 11417746]

10. Patchell RA, Tibbs PA, Regine WF, Payne R, Saris S, Kryscio RJ, et al. Direct decompressive surgical resection in the treatment of spinal cord compression caused by metastatic cancer: a randomised trial. Lancet. 2005; 366:643–648. [PubMed: 16112300]
11. Taahashi M, Ogawa J, Kinoshita Y, Takakura M, Mochizuki K, Satomi K. Experimental study of paraplegia caused by spinal tumors: an animal model of spinal tumors created by transplantation of VX2 carcinoma. Spine J. 2004; 4:675–680. [PubMed: 15541702]
12. Tatsui H, Onomura T, Morishita S, Oketa M, Inoue T. Survival rates of patients with metastatic spinal cancer after scintigraphic detection of abnormal radioactive accumulation. Spine. 1996; 21:2143–2148. [PubMed: 8893440]
13. Ushio Y, Posner R, Posner JB, Shapiro WR. Experimental spinal cord compression by epidural neoplasm. Neurology. 1977; 27:422–429. [PubMed: 558545]

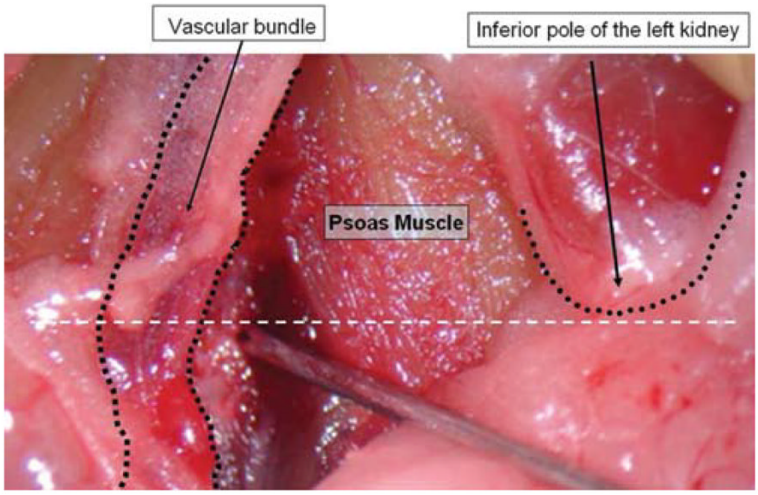

Fig. 1.

Intraoperative photograph showing landmarks for exposure of the L-3 VB. The retroperitoneal space was opened between the left kidney and the vascular bundle, exposing the left psoas muscle. The L3–4 intervertebral disc is located in a plane caudal to the inferior pole of the left kidney *(white dashed line)*.

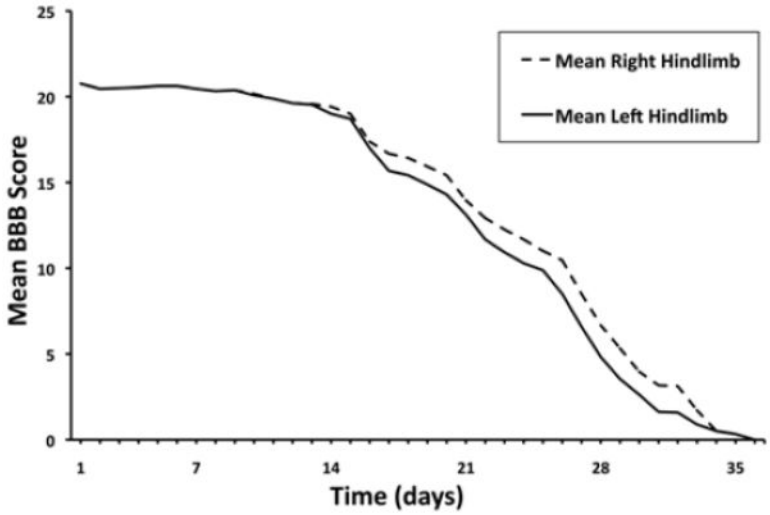

Fig. 2.

Graph depicting the mean BBB scores of the mice over time. The mean BBB score was calculated each day and plotted against time to show the trend in neurological impairment. These daily averages are distinct from the median times to each of the 4 milestones shown in Table 2, which were determined using the Kaplan-Meier method.

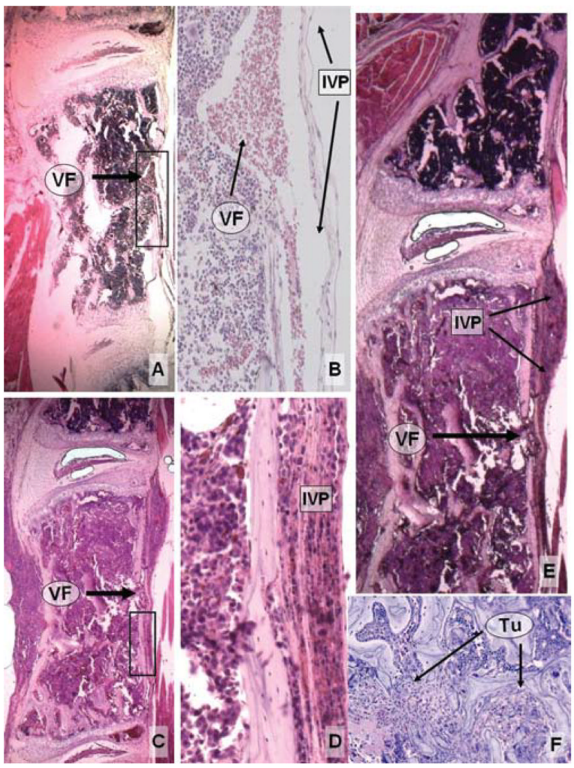

Fig. 3.

Photomicrographs of histological specimens depicting the invasion of PC-14 implants into the spinal canal. A: Sagittal section of a normal vertebral level demonstrating the muscle layer anterior to the VB and a normal venous foramen with a patent IVP. B: Higher magnification of the *inset* in panel A, demonstrating red blood cells within a normal venous foramen and IVP. C: Section showing PC-14 cells infiltrating the VB 7 days after implantation. Tumor cells are seen within the venous foramen and occluding the IVP. D: Higher magnification of the *inset* in panel C, demonstrating tumor cells occluding the IVP. E: Sagittal section demonstrating a normal level (*upper part* of the panel) containing healthy bone marrow, and a level completely colonized by PC-14 cells (*lower part* of the panel). Note the extension of tumor cells through the venous foramen and IVP, forming an early epidural mass. F: Tumor cells initially replace the bone marrow, and only gradually alter the architecture of the trabecular bone. H & E, original magnification × 50 (A, C, and E); × 200 (B and D); × 100 (F). Tu = tumor; VF = venous foramen.

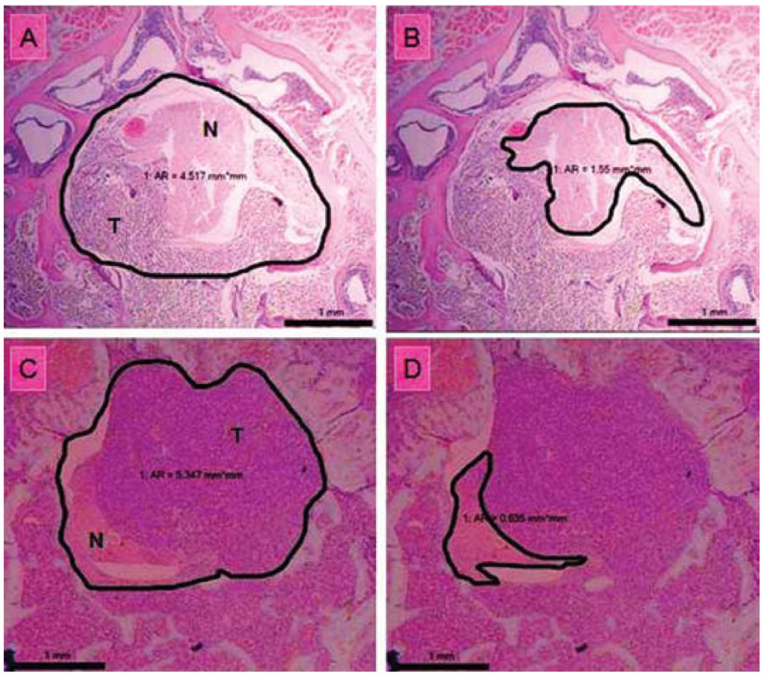

Fig. 4.

Photomicrographs of histological specimens depicting the method used to calculate the neural/canal ratio. A: Axial section of a specimen harvested 14 days after tumor implantation, with the area of the spinal canal outlined. B: Specimen from panel A, with the area of the spinal cord and nerve roots outlined. Note that the tumor is deforming the round contour of the neural elements. C: Axial section of a specimen harvested 28 days after tumor implantation, with the area of the spinal canal outlined. D: Specimen from panel C, with the area of the spinal cord and nerve roots outlined. Note that the epidural tumor is severely compressing the neural elements. H & E, original magnification × 50. AR = area (in square millimeters); N = neural elements; T = tumor.

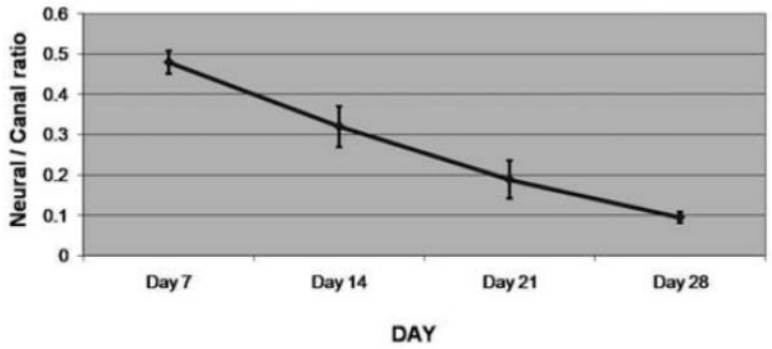

Fig. 5.

Graph depicting the mean neural/canal ratio, with the SEM represented by *error bars*, at 7, 14, 21, and 28 days after tumor implantation. The ratio decreases from Day 7 to Day 28, corresponding to progressive tumor infiltration into the spinal canal and compression of the neural elements.

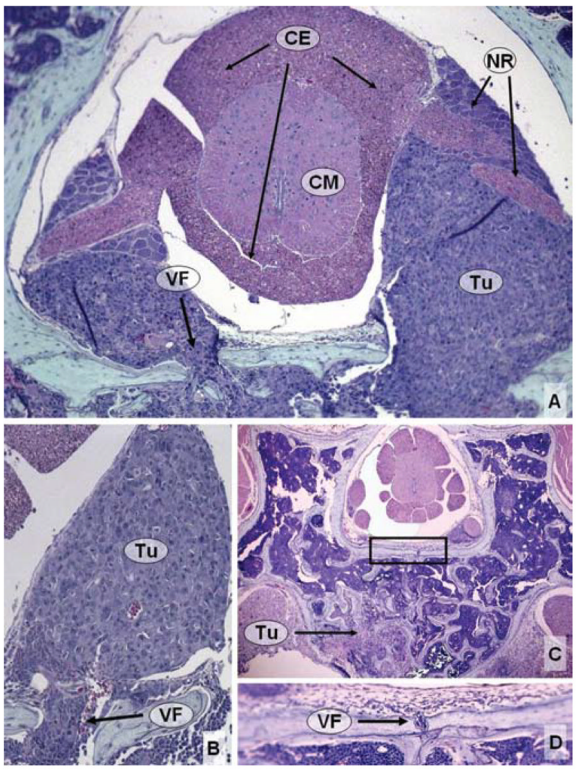

Fig. 6.

Photomicrographs showing histological specimens obtained at Day 7 after tumor implantation. A: In this specimen, tumor is infiltrating the epidural space, surrounding the nerve roots, but causing no mass effect on the spinal cord. B: Note that the venous foramen is invaded by tumor cells, enabling access to the epidural space. C: In this axial cut, the tumor is less advanced. There is partial infiltration of the VB. D: Higher magnification of the *inset* in panel C, showing a small venous foramen crossing the posterior cortex of the vertebra. These channels provide an access route for tumor cells in the marrow to reach the epidural space. H & E, original magnification × 100 (A and B); × 50 (C); × 200 (D). CE = cauda equina; CM = conus medullaris; NR = nerve root.

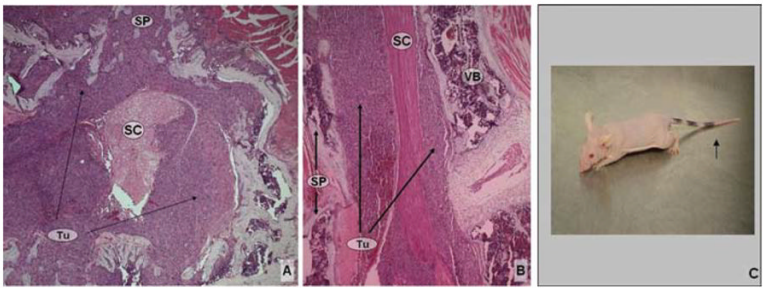

Fig. 7.

Photomicrographs showing histological specimens obtained at Day 14 after tumor implantation, and photograph of a mouse at milestone 1. A: Tumor cells are infiltrating the VB, posterior elements, and epidural space, with mild circumferential spinal cord compression. B: Sagittal section cut at the level caudal to the tumor implantation, demonstrating the extensive epidural disease. H & E, original magnification × 50 (A and B). C: Photograph of mouse obtained at neurological examination, which at this time typically reveals tail dragging *(arrow)*. SC = spinal cord; SP = spinous process.

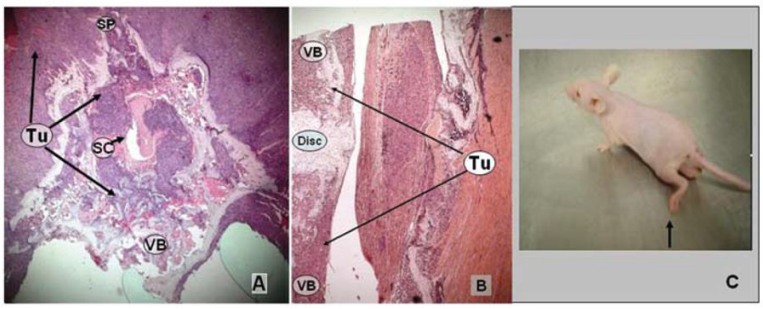

Fig. 8.

Photomicrographs showing histological specimens obtained at 21 days after tumor implantation, and photograph of a mouse at milestone 2. A: Tumor is infiltrating the VB, posterior elements, and epidural space with severe circumferential spinal cord compression. B: Sagittal section cut at a level caudal to the site of tumor implantation, showing infiltration into the adjacent VBs. H & E, original magnification × 50 (A and B). C: Photograph of mouse obtained at neurological examination; at this stage, functional assessment of the animals is expected to reveal dorsal stepping *(arrow)*. Disc = intervertebral disc.

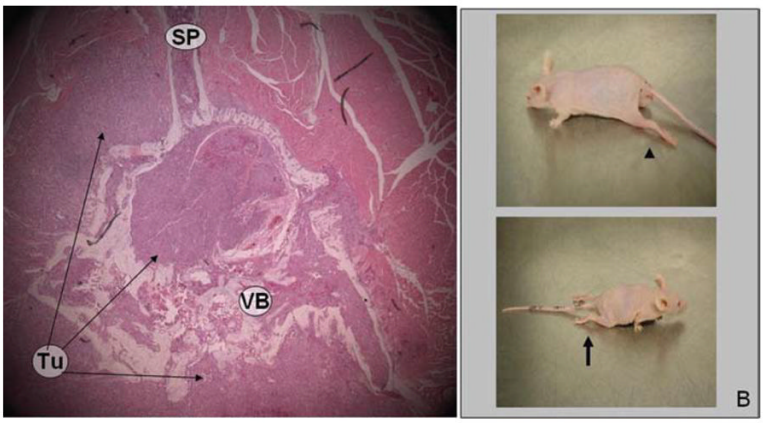

Fig. 9.

Photomicrograph showing histological specimens obtained at 28 days after tumor implantation, and photographs of mice at milestones 3 and 4. A: Tumor has filled the spinal canal and obliterated the spinal cord. H & E, original magnification × 50. B: Photographs of mice obtained at neurological examination; the predicted neurological findings at this stage are hindlimb sweeping *(arrowhead)* progressing rapidly to paralysis *(arrow)*.

TABLE 1

Key BBB milestones, with clinical correlation

BBB Scores	Clinical Milestone
21–19	1: normal to tail dragging
19–14	2: tail dragging to dorsal stepping
14–8	3: dorsal stepping to hindlimb sweeping
≤8	4: hindlimb sweeping to paralysis

TABLE 2

Timeframe for occurrence of key neurological events (milestones) in a mouse model of spinal metastasis

	Median Days to Milestone (95% CI)			
Affected Limb	**Tail Dragging**	**Dorsal Stepping**	**Hindlimb Sweeping**	**Paralysis**
rt hindlimb	12 (10.8–13.2)	23 (20.6–25.4)	28 (27.1–28.9)	30 (28.1–31.9)
lt hindlimb	12 (10.8–13.2)	21 (19.4–22.6)	26 (23.6–28.4)	29 (27.6–30.4)

TABLE 3

Histological features of tumor progression in a mouse model of spinal metastasis *

	Days After Tumor Implantation			
Feature	**7**	**14**	**21**	**28**
infiltration of VB & posterior elements	partial	complete	complete	complete
extension to adjacent levels	no	epidural	epidural & osseous	epidural & osseous
nerve root compression	partial	complete	complete	complete
spinal cord compression	none	mild	severe	obliterated
mean neural/canal ratio (± SEM)	0.48 ± 0.03	0.32 ± 0.05 *	0.19 ± 0.05 †	0.09 ± 0.01 †

* $p = 0.04$.

† $p < 0.001$ compared with Day 7.